Nanocrystallized ceria-based coatings prepared by electrochemistry on TA6V titanium alloy

Laurent Arurault [a,*], Barbara Daffos [a], François X. Sauvage [b]

[a] *Centre Interuniversitaire de Recherche et d'Ingénierie des Matériaux (CIRIMAT), UMR 5085, CNRS/INPT/UPS , Laboratoire de Chimie des Matériaux Inorganiques et Energétiques (LCMIE), Université Paul Sabatier, 118 Route de Narbonne, F-31062 Toulouse Cedex 09, France*

[b] *LASIR-HEI, CNRS UMR 8516, 13 Rue de Toul, F-59046 Lille Cedex, France*

Abstract

Nanocrystallized ceria-based coatings were prepared on TA6V titanium alloy by using a three-step procedure: substrate pre-treatment, electrochemical impregnation and final heat treatment.

UV–vis and Raman *in situ* spectroscopies performed at the substrate interface during the electrochemical impregnation, showed experimentally for the first time that the interfacial deposit is made up of cerium hydroxide, incorporating also water molecules and nitrate ions coming from the electrolyte. Thermogravimetric analysis indicated also that the composition of the coating after the impregnation is given by the global formula $CeO_2 \cdot 3.4H_2O$, while XRD analysis revealed that ceria with cubic fluorite crystalline structure is finally produced.

Different preparation conditions were studied in view to control the nanosize of the supported ceria crystallites. It appeared that the final heat treatment is the most efficient operational parameter for the tuning of the particle size, that it can be thus well controlled from 5 to 30 nm between 300 and 700 °C.

Keywords: A. Oxides; B. Crystal growth; C. Raman spectroscopy; C. X-ray diffraction

1. Introduction

Nanocrystalline ceria (CeO_2) particles have been recently extensively studied because of their very interesting properties, especially for technological applications such as energy storage [1,2] and catalysis [3–5] due to its capacity for oxygen storage or release. Various techniques are used to obtain ceria nanopowders, such as microwave assisted heating technique [6,7], precipitation method [8–10], combustion method [11], microemulsion technique [12–14], hydrothermal precipitation [15,16] and flux method [17]. The objectives of all these research works are to prepare weakly agglomerated nanocrystalline powders, with low contamination, at low preparation costs, controlling the particle size and their morphology.

The electrochemical impregnation (ECI) will be here chosen for the coatings preparation since this method offers many attractive advantages such as a limited cost, an easy control of the deposit characteristics and the possibility to obtain ceria directly onto the metal substrate.

* Corresponding author. Tel.: +33 5 61 55 61 48; fax: +33 5 61 55 61 63.
E-mail address: arurault@chimie.ups-tlse.fr (L. Arurault).

doi:10.1016/j.materresbull.2007.07.019

Production of ceria by ECI method was firstly exposed by Switzer [18–20] and then developed by various other authors [21–26] on different substrates such as aluminium or steel alloys, and even glass coated with SnO_2 [27] but never until now on titanium substrate. Moreover, despite these previous studies, the reactional mechanisms of the ceria coatings formation are not yet well established and remain in discussion [23,28].

The main aim of the present study will be to prepare, by electrochemical impregnation, nanocrystallized ceria-based coatings on TA6V titanium alloy substrate. In particular, the reactional mechanisms of the ceria formation will be investigated by *in situ* characterizations, while dehydration and crystalline growth processes will be studied in view to finally control the nanosize of the crystallized supported ceria.

2. Experimental

2.1. Preparation procedures

The preparation followed a three-step process: (1) surface preparation of the metallic substrate, (2) electrochemical impregnation and (3) final heat treatment.

The samples were disks (diameter 14 mm) of Ti–6%Al–4%V titanium alloy. During the first step, they were at first polished mechanically (grade 600), then cleaned for 5 min at room temperature in an acetone–ethanol (50–50%, v/v) mixture, and finally etched during 10 min at room temperature in an aqueous solution containing hydrofluoric acid (2 vol.%).

The operational parameters of the electrochemical impregnation (second step) were chosen on the basis of our previous study [23]. However the main difference is that the electrochemical device is in this study a single cell, whereas previously the electrochemical cell was made up of two compartments (anodic and cathodic) divided by a diaphragm. The sample was used as the cathode and a platinum plate was the counter-electrode, while the electrolyte is a cerous nitrate aqueous solution $Ce(NO_3)_3{\cdot}6H_2O$ (0.1 M; pH_{bulk} 2.9) at room temperature. All the samples were prepared in the optimal conditions corresponding to a cathodic current density of -40 A m^{-2} for 10 min. After impregnation, the sample was rinsed with deionised water and dried in air.

The final step was a heat treatment in a dynamic oxidizing atmosphere (100 mL/min, 80 vol.%–20%O_2), according to the following temperature program: from room temperature up to 700 °C at a rate of 7.9 °C/min, then 1 h at 700 °C and then down to room temperature at a rate lower than 7.9 °C/min.

For comparison, a solution based on cerium hydroxide was also prepared by precipitating the previous cerous nitrate solution (0.1 mol/L, $V = 25$ mL) with NaOH ($C = 1.014$ mol/L, $V = 7.56$ mL).

2.2. Characterization techniques

X-ray diffraction (XRD) analysis was performed with a Bragg Brentano (Seifert XRD 3003TT) generator with copper anticathode ($K_\alpha = 1.5418$ Å). All diffraction profiles were obtained by varying 2θ from 10° to 100° with a step scan increment of 0.05°. The time step was 15 s. Peaks were finally identified by using the Powder Diffraction Files, Joint Committee on Powder diffraction Standards, ASTM, Philadelphia, PA, 1998, card 34-0.394.

Moreover, the microstructure of polycrystalline materials could be characterized from the X-ray diffraction patterns by using the Williamson–Hall technique (Appendix A), fitting the individual peaks with a pseudo-Voigt function in order to obtain both the average crystallite size and microstrain.

The coatings dehydration process was studied by thermogravimetric analysis (TG) in air from 25 to 1000 °C at a heating rate of 3 °C/min, by using a SETARAM instrument (Model TGDTA 92 equipped with a platinum crucible).

The coatings thickness was evaluated using a scanning electron microscopy (SEM JEOL instrument, model JSM-35 CF).

The *in situ* Raman interfacial measurements were performed with a Labram (DILOR) microspectrometer equipped with a He–Ne laser ($\lambda = 632.8$ nm, 2 mW) and a ''notch'' filter at 600 nm. The Raman signal was collected through the objective of a microscope ($G = 50\times$) and a holographic monochromator (1800 lines/mm). It finally fell on a CCD detector (Wright) cooled at -30 °C. Each spectrum was measured over 60 s, which ensured a satisfactory signal-to-noise ratio.

The UV–vis spectra were recorded *in situ* on a Tidas 2 diode array multichannel spectrometer (J&M Company, Germany), equipped with a fiber optics device in order to collect the spectra from the remote spectroelectrochemical

cell. The light sources were deuterium (UV) and tungsten halogen (visible) lamps. The overall wavelength range was 190–1020 nm (the spectra were recorded between 200 and 900 nm). The detector had 1024 diodes, thus allowing a spectral resolution of *ca.* 0.8 nm. The spectrometer was operated through the Spectralys software running on a PC. This multitask program handled the parameters of the instrument, the collection of the spectra and the processing of the data. The spectra were collected at regular time intervals (5–10 s) over an integration period of *ca.*1 s.

All reagents were analytical grade products (PROLABO) and the aqueous electrolyte solutions were obtained by using deionised water.

3. Results and discussion

The following results and discussion are linked according to the various steps of the preparation procedure. At first, *in situ* characterizations were performed at the substrate interface during the electrochemical impregnation in view to clarify the formation mechanisms. In the second part, different preparation conditions, especially the finishing heat treatment conditions, were studied and correlated to the nanosize of the crystallized supported ceria.

3.1. Study of the intermediate coating during the impregnation step

3.1.1. Interfacial UV–vis spectroscopy

Fig. 1 shows the UV–vis spectrum of the coating formed on the cathode as a function of the duration of the electrochemical impregnation. A single peak located at 340 nm clearly increases with the impregnation time, i.e. the formation of the deposit. As a comparison, Fig. 2 also presents the spectrum of the cerium hydroxide obtained by the precipitation procedure. This latter spectrum also reveals a typical peak around 340 nm, thus proving the comparable composition of the two compounds, and showing clearly the precipitation of a cerium hydroxide on the electrode surface during the electrochemical impregnation.

3.1.2. Interfacial Raman spectroscopy

The *in situ* Raman spectrum of the interfacial deposit (Fig. 3) displays four bands at 460, 750, 1090 and 1500 cm^{-1}. This latter is very weak, broad and rather ill-defined. Since its intensity slightly decreased with time (i.e. drying effect of the sample under the laser beam?) it could be due to water molecules. On the other hand, this area also corresponds to weak N–O vibrations. Accordingly, this band cannot be assigned with certainty.

In order to identify the other peaks, the following three supplementary compounds were studied:

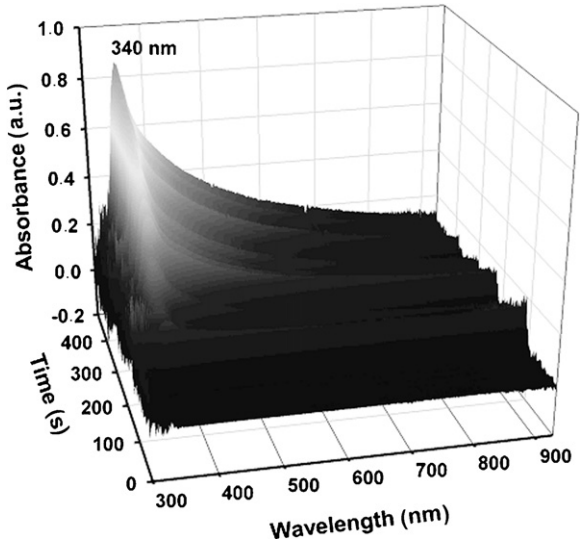

Fig. 1. *In situ* UV–vis spectrum of the interfacial cathodic deposit obtained during the electrochemical impregnation.

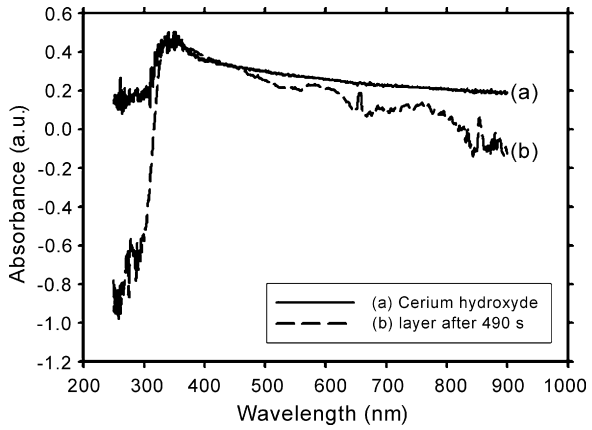

Fig. 2. Comparison of the *in situ* UV–vis spectra of the interfacial cathodic deposit obtained during the electrochemical impregnation and the cerium hydroxide obtained by the coprecipitation.

- cerous nitrate $Ce(NO_3)_3{\cdot}6H_2O$ powder;
- ceria CeO_2 powder;
- the previous solution of cerium hydroxide obtained by precipitation.

Beside the peak located around 1500 cm^{-1}, the spectrum of cerous nitrate displays two additional bands at 750 (very weak) and 1090 cm^{-1} (strong), whereas two other peaks appear at 460 and 1090 cm^{-1} with the cerium hydroxide. The Raman spectrum of ceria powder shows a single additional peak located at 465 cm^{-1}.

These results reveal that the peak located at 460 cm^{-1} is clearly associated to the Ce–O link, in good agreement with previous studies [24,29–31], the hydroxyl link being difficult to reveal in this case, due to the aqueous solvent. On the contrary, the other two peaks (750, 1090 cm^{-1}) are mainly explained by the nitrate ions.

3.1.3. Formation mechanisms

In these experimental impregnation conditions (aerated aqueous solution of cerous nitrate of $pH_{bulk} < 4$), the coating formation results from complex mechanisms at the cathode, based on the interfacial pH increase generated by reduction reactions. At first, the nitrate ions from the solute could be reduced into ammonium ions according to the following reactions [32]:

$$NO_3^- + 10H^+ + 8e \rightarrow NH_4^+ + 3H_2O \quad (1)$$

$$NO_3^- + 7H_2O + 8e \rightarrow NH_4^+ + 10OH^- \quad (2)$$

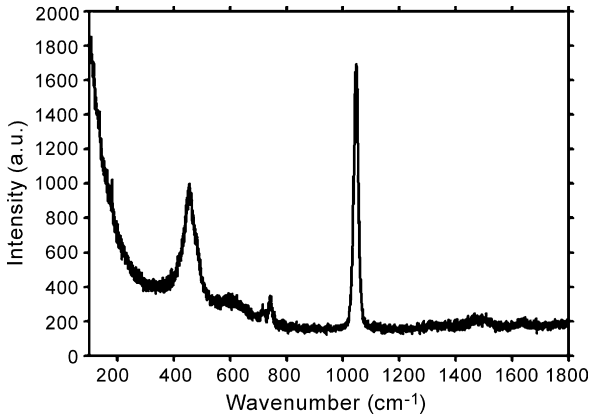

Fig. 3. *In situ* Raman spectrum of the interfacial cathodic deposit obtained during the electrochemical impregnation.

Furthermore, water, H_3O^+ ions or dissolved O_2 in the solvent could be also reduced [28] according to:

$$2H_3O^+ + 2e \rightarrow H_2 + 2H_2O \quad (3)$$

$$2H_2O + 2e \rightarrow H_2 + 2OH^- \quad (4)$$

$$O_2 + 2H_2O + 4e \rightarrow 4OH^- \quad (5)$$

$$O_2 + 2H_2O + 2e \rightarrow 2OH^- + H_2O_2 \quad (6)$$

In all cases, the consumption of H_3O^+ ions in reactions (1) and (3) or the formation of OH^- ions in reactions (2), (4)–(6) induce under the cathodic polarization a pH increase in the double layer at the cathode interface, in spite of the low pH value (pH_{bulk} 2.9) of the bulk electrolyte. This local pH increase induces then on the substrate surface the precipitation of metallic cations hydroxides with low solubility product. However the exact composition of the hydroxides in these experimental conditions are not determined until now, especially by experimental analysis techniques. Previous studies about electrochemical or chemical precipitation, claimed indeed, on the base on only theoretical considerations, the existence, in very alkaline and aerated conditions, of various possible species, such as $Ce(OH)_3$ [33], $Ce(OH)_4$ or $CeO_2{\cdot}nH_2O$ [10], as well as the intermediate compounds $Ce(OH)_2^{2+}$ [28,34], $Ce(OH)_x(OOH)_{4-x}$ [15] and $[Ce(OH)_x(H_2O)_y]^{(4-x)+}$ [7,20]. The corresponding formation mechanisms are possibly chemical or electrochemical. For example, the formation of cerous hydroxide $Ce(OH)_3$ [33] and/or the formation of the ionic species $Ce(OH)_2^{2+}$ [28] could occur according to:

$$Ce^{3+} + 3OH^- \rightarrow Ce(OH)_3 \quad (7)$$

$$4Ce^{3+} + O_2 + 4OH^- + H_2O \rightarrow 4Ce(OH)_2^{2+} \quad (8)$$

The direct formation of ceria CeO_2 [29] in solution is even supposed:

$$Ce(OH)_3 \rightarrow CeO_2 + H_3O^+ + e \quad (9)$$

$$Ce(OH)_2^{2+} + 2OH^- \rightarrow CeO_2 + 2H_2O \quad (10)$$

Furthermore, the specificity of our experimental device, i.e. an electrochemical cell included a single compartment, allow the possibility at the anode to oxidize the cerous ions Ce(III) into ceric ions Ce(IV) ($E^0_{Ce(IV)/Ce(III)} = +1.46\,V/HNE$), inducing the formation of more stable compounds such as $Ce(OH)_4$ and $CeO_2{\cdot}nH_2O$.

So this study shows experimentally for the first time, using two different *in situ* characterizations, that in these operational conditions the intermediate compounds during the impregnation step are clearly cerium hydroxides. Moreover, this study clearly shows experimentally also for the first time that the ECI coatings incorporate not only water molecules but also nitrate ions coming from the impregnation electrolyte. This adsorption of nitrate ions could be perhaps explained by the positive surface charge of the primary hydrous ceria particles, following the example of the previous study [10] about the hydrous ceria obtained in an acidic solution during a two-stage precipitation chemical process.

3.2. Study of the final coating after the heat treatment

3.2.1. Calcination and crystallization of the coatings

The coating obtained at the end of the impregnation (the second step of the preparation process) are 15 ± 2 μm thick, homogenous, adherent and without macrocracks. Moreover, XRD patterns before the heat treatment (Fig. 4) reveal broad peaks, probably indicating an amorphous phase with small size particles. On the contrary, the XRD patterns obtained after the heat treatment (Fig. 4) exhibit well-defined and intense diffraction peaks corresponding to the (1 1 1), (2 0 0), (2 2 0), (3 1 1) ceria crystallographic planes. Moreover some additional low peaks can be attributed [35] to the titanium alloy surface and probably to the rutile phase at 700 °C rather than the anastase one, these substrate peaks remaining however very low in comparison with the ceria peaks because the coatings are here quite thick. So, the calcination of the coatings induces the ultimate formation of ceria, the most stable cerium oxide ($\Delta_f G^\circ_{CeO_2} = -1024.6\,kJ/mol$ [36]). Considering that the crystalline structure of ceria is the cubic fluorite system [15], the experimental cell parameter is here equal to 5406 Å, result in good agreement with previous works [18,19].

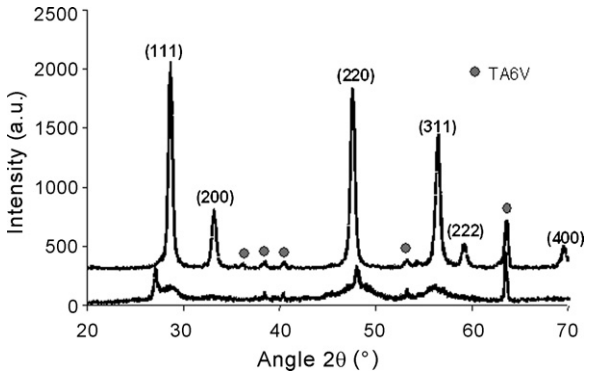

Fig. 4. XRD diagrams obtained after impregnation (−40 A m^{-2}, 10 min at room temperature) (bottom diagram) and after final heat treatment (1 h at 700 °C) (upper diagram).

According to the thermogravimetric analysis (Fig. 5), this calcination induces a global weight loss of 25% occurring mainly in the 25–400 °C temperature range. A first stage up to about 120 °C can be mainly attributed to the evaporation of the physically adsorbed water [25,26,37], while the removal of nitrate ions can be assigned at a temperature about 200 °C [36]. Above 400 °C, the low weigh decrease can be assigned to the removal of the chemisorbed water [37]. Considering dehydration only, the composition of the coating after the impregnation step is given, from the TG results, by the global formula $CeO_2 \cdot 3.4H_2O$, in good agreement with previous work on copper and stainless steel substrates [23,38], showing thus that the metallic substrate has no direct influence on the formation mechanisms.

3.2.2. Influence of the thermal treatment step on the nanosize tuning

Fig. 6 shows the XRD patterns obtained at various temperatures (100–700 °C) of the final heat treatment. The peaks become thinner and increase with temperature during the final heating. By using the Williamson–Hall technique, fitting the individual peak by a pseudo-Voigt function, the average crystallite size and microstrain could be obtained plotting β^* as a function of d^* (Appendix A). All the slopes are weak (Fig. 7) attesting that the crystals contain few microdistortions and have a spherical shape. Moreover, Fig. 8 reveals that the crystallite size remains low and constant in the 25–300 °C temperature range, while in the 300–700 °C temperature range this parameter increases from 5 to 30 nm, steep increase probably linked to a decrease of the corresponding specific surface area [35,39]. These supported crystallite sizes, calculated from the DRX analysis, are similar in comparison with the previous study [39] showing the effect of calcination (20–800 °C) on the particles size (respectively from 3.18 to 34.4 nm) of ceria ultrafine particles obtained by solid state reactions. So the size of the ceria-supported crystallites could be easily controlled in the temperature range as extensive as 300–700 °C, due to the refractory properties of the titanium substrate. In these conditions of heat treatment, i.e. up to 700 °C, there is probably a simultaneous decrease of the surface area due to the ceria crystallites growth but without sintering phenomenon because it is currently established that the pure ceria (without sintering promoters) is difficult to densify below 750 °C [19,37,40].

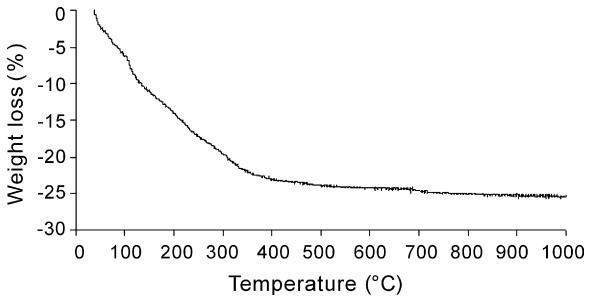

Fig. 5. Thermogravimetric analysis of the hydrated deposit just after the electrochemical impregnation (−40 A m^{-2}, 10 min at room temperature).

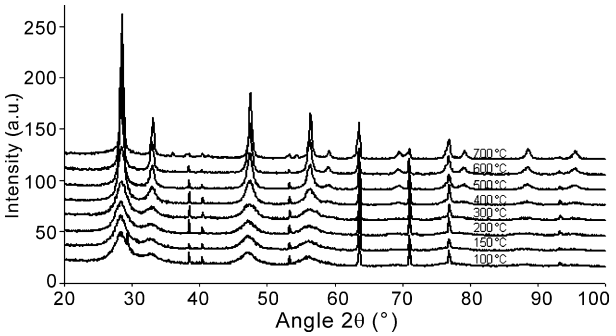

Fig. 6. XRD patterns obtained at different temperatures (100–700 °C) of the final heat treatment.

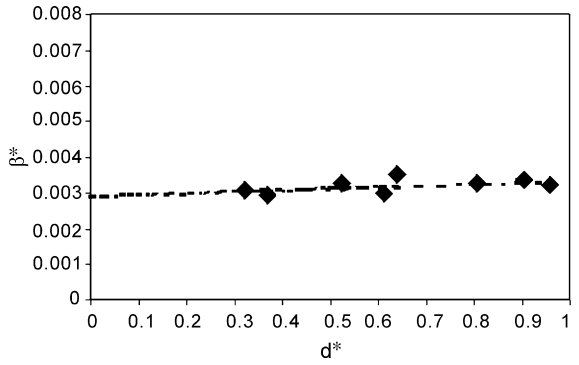

Fig. 7. Determination of the average crystallite size and microstrain by the Williamson–Hall technique for the ceria sample prepared at -20 A m^{-2}.

3.2.3. Influence of the impregnation step on the nanosize tuning

Fig. 9 summarizes the crystallite size, obtained by simulation peak by peak of DRX patterns, as a function of the current density of the impregnation step, the final heat treatment remaining constant (1 h at 700 °C). The results show that the crystals contains few microdistortions, while the final crystallite size decreases from 35 to 26 nm for corresponding current density from -20 to -50 A m^{-2}. This final change of the crystallite size could be in fact explained by the electrocrystallization phenomenon, especially by the nucleation and growth process that is the rate-determining step of the impregnation of cerium oxide films [41]. For high current density, the nucleation rate on the titanium electrode exceeds the growth of the cerium (oxy-)hydroxides nuclei, while the nuclei growth rate predominates at lower current density [42]. From this perspective, an increase of the absolute value of the current density (from -20 to -50 A m^{-2}) during the impregnation step induces so a decrease of the final size of ceria crystallites (from 35 to 26 nm) for the same heat treatment. Moreover a previous study [20] about the preparation of similar ceria coatings on 430 stainless steel substrate showed that the crystallite size varies from 18 to 6 nm when the

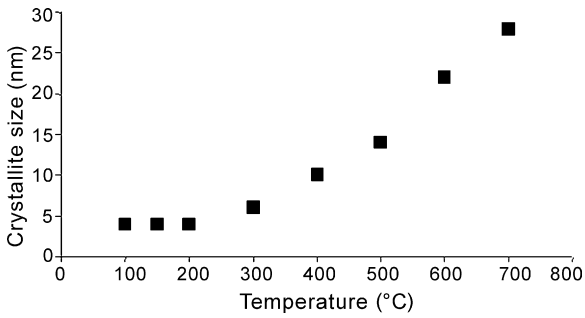

Fig. 8. Ceria crystallite size calculated for different temperatures (100–700 °C) of the final heat treatment.

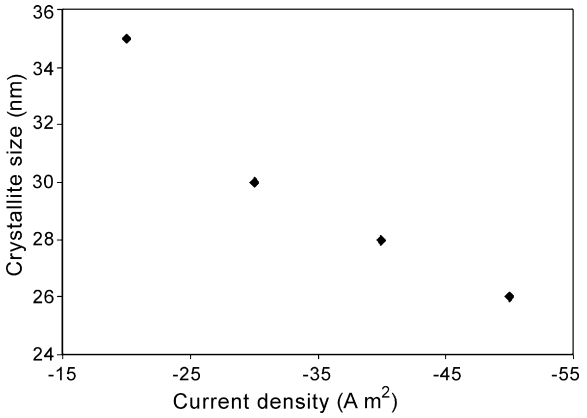

Fig. 9. Effect of current density on the crystallite size of CeO_2 constituting coating; final heat treatment: 700 °C.

applied current density increased from -5 to -30 A m^{-2}, the deposits being only dried for 24 h in air at room temperature. The differences of crystallite sizes between the two studies could be then explained mainly by the higher temperature in the final heat treatment rather than the current density changes during the impregnation step. So the current density is also another easy way to control the ceria crystallite nanosize, but it appears less efficient compared with the wide control of the crystallite size (5–30 nm) through the changes of the final heat treatment (300–700 °C).

4. Conclusions

The aim of this work was to prepare nanocrystallized ceria-based coatings on TA6V titanium alloy. The preparation involved conditioning the substrate, electrochemically impregnating it with cerium oxy-hydroxides and finally subjecting it to heat treatment to dehydrate the deposit leaving a coat of nanocrystallized ceria.

At first, *in situ* characterizations (UV–vis and Raman *in situ* spectroscopies) were performed at the substrate interface during the electrochemical impregnation. This study showed, for the first time experimentally, that the deposit is mainly composed by cerium hydroxide, also incorporating water molecules and nitrate ions coming from the impregnation electrolyte.

In the second part, the final characteristics of the coating were studied as a function of different preparation conditions. XRD analysis showed first that the final coating is made up of ceria with cubic fluorite crystalline structure, while thermogravimetric results indicated that the composition of the coating after the impregnation step is given by the global formula $CeO_2{\cdot}3.4H_2O$. By using the Williamson–Hall technique, XRD results showed that the crystallite nanosize can be easily controlled by the current density during the impregnation. But the impact of the heat treatment is larger on the particle size than the current density. Thus the nanosize of the crystallized supported ceria remains low and constant in the 25–300 °C temperature range, while it could be well controlled from 5 to 30 nm in the 300–700 °C temperature range, without sintering phenomenon.

So this study showed the possibility, using a low cost process, to obtain thick, homogenous, adherent ceria coatings supported on a titanium alloy, i.e. a refractory metallic substrate. Moreover, the operational parameters of the process allowed to control the hydration rate as well as the crystallite size in view to adjust the active surface and to increase the chemical stability of these coatings. The forthcoming applications are at present to use the thick ceria coatings to improve the chemical inertia of parts against the corrosion in very aggressive medium at high temperatures or to prepare active catalytic materials, such as Pt/CeO_2, with high contact surface for the oxidation of carbon monoxide.

Acknowledgements

This study was financially supported for a part by the French ‘‘Ministère de la Recherche’’ through the APROSUTIS-RMNP program. The authors express their thanks to P. Lenormand for his helpful discussions concerning the Williamson–Hall technique. The help of A. Latacz, S. Picque, M. Sterckeman and R. Tassot for the spectroelectrochemical measurements is gratefully acknowledged.

Appendix A. Williamson–Hall technique fitting by a pseudo-Voigt function

From XRD patterns, the integral width of the peaks (β) can be to connect to the apparent size of the crystals and their internal microdistorsion [43] according to:

$$\beta = \frac{\lambda}{L\cos\theta} \quad \text{(broadening with the size changes)}$$

and

$$\beta = \eta\tan\theta \quad \text{(broadening induced by the lattice distorsion)}$$

If β_P is the true width, while β^T and β^D are the widths related on the size and the lattice distortion, respectively, then one can write:

$$\beta_P = \beta^T + \beta^D$$

and thus $\beta = \lambda/(L\cos\theta) + \eta\tan\theta$ or $(\beta\cos\theta)/\lambda = 1/L + \eta(\sin\theta/\lambda)$.

According to the Bragg's law:

$$\frac{\sin\theta}{\lambda} = \frac{1}{2d} = \frac{d^*}{2}$$

So the relation becomes:

$$\beta^* = \frac{1}{L} + \left(\frac{\eta}{2}\right)d^* \quad \text{with} \quad \beta^* = \frac{\beta\cos\theta}{\lambda}$$

Plotting β^* as a function of d^*, a line is typically obtained, giving both the crystals size (from the origin) and their microdistortions (from the slope). In particular, a weak slope attests that the crystal have a spherical form and contains few microdistortions.

References

[1] D.L. Marricle, T.E. Sawrr, S. Karavolis, Solid State Ionics 52 (1992) 173.
[2] Y. Xiong, K. Yamaji, N. Sakai, H. Negishi, T. Horita, H. Yokokawa, J. Electrochem. Soc. 148 (2001) E489.
[3] S. Sharma, S. Hilaire, J.M. Vohs, R.J. Gorte, H.-W. Jen, J. Catal. 190 (2000) 199.
[4] S. Enzo, F. Delogu, R. Frattini, A. Primavera, A. Trovarelli, J. Mater. Res. 15 (7) (2000) 1538.
[5] M. Ozawa, J. Alloys Compd. 275–277 (1998) 886.
[6] A. Bonamartini Corradi, F. Bondioli, A.M. Ferrari, T. Manfredini, Mater. Res. Bull. 41 (2006) 38.
[7] H. Yang, C. Huang, A. Tang, X. Zhang, W. Yang, Mater. Res. Bull. 40 (2005) 1690.
[8] T.J. Kirk, J. Winnick, J. Electrochem. Soc. 140 (1993) 3494.
[9] E. Muccillo, R. Rocha, S. Tadokoro, J. Rey, R. Muccillo, M. Steil, J. Electroceram. 13 (2004) 609.
[10] F. Zhang, S.-P. Yang, H.-M. Chen, X.-B. Yu, Ceram. Int. 30 (2004) 997.
[11] R.D. Purohit, B.P. Sharma, K.T. Pillai, A.K. Tyagi, Mater. Res. Bull. 36 (2001) 2711.
[12] Y.J. He, B. Yang, G. Cheng, Mater. Lett. 57 (2003) 1880.
[13] J.-S. Lee, J.-S. Lee, S.-C. Choi, Mater. Lett. 59 (2005) 395.
[14] S. Patil, S.C. Kuiry, S. Seal, R. Vanfleet, J. Nanoparticle Res. 4 (2002) 433.
[15] J.-S. Lee, S.-C. Choi, Mater. Lett. 58 (2004) 390.
[16] Y.C. Zhou, M.N. Rahaman, J. Mater. Res. 8 (7) (1993) 1680.
[17] F. Bondioli, A. Bonamartini Corradi, C. Leonelli, T. Manfredini, Mater. Res. Bull. 34 (14/15) (1999) 2159.
[18] J.A. Switzer, Am. Ceram. Soc. Bull. 66 (10) (1987) 1521.
[19] Y. Zhou, R.J. Phillips, J.A. Switzer, J. Am. Ceram. Soc. 78 (4) (1995) 981.
[20] Y. Zhou, J.A. Switzer, J. Alloys Compd. 237 (1996) 1.
[21] B.R.W. Hinton, D.R. Arnott, N.E. Ryan, Mater. Forum 9 (3) (1986) 162.
[22] V. Poulain, PhD Thesis, Faculté Polytechnique de Mons, Belgium, 1999 (in French).
[23] L. Arurault, P. Monsang, J. Salley, R.S. Bes, Thin Solid Films 466 (2004) 75.
[24] J. Creus, F. Brezault, C. Rebere, M. Gadouleau, Surf. Coat. Technol. 200 (14/15) (2005) 4636.
[25] I. Zhitomirsky, A. Petric, Mater. Lett. 40 (1999) 263.
[26] I. Zhitomirsky, A. Petric, Ceram. Int. 27 (2001) 149.
[27] M. Izaki, M. Ishikawa, M. Inoue, in: K.R. Hebert, R.S. Lillard, B.R. MacDougall (Eds.), Oxide Films, Electrochemical Society Publishing, PV 2000-4, Toronto, Canada, 2000, p. 333.
[28] A.J. Aldykiewicz Jr., A.J. Davenport, H.S. Isaacs, J. Electrochem. Soc. 143 (1) (1996) 147.

[29] I. Kosacki, T. Suzuki, H.U. Anderson, P. Colomban, Solide State Ionics 149 (2002) 99.
[30] J.E. Spanier, R.D. Robinson, F. Zhang, S.-W. Chan, I.P. Herman, Phys. Rev. B: Condens. Matter Mater. Phys. 64 (2001) 245407.1.
[31] S. Wang, W. Wang, J. Zuo, Y. Qian, Mater. Chem. Phys. 68 (2001) 246.
[32] Y. Matsumoto, H. Adachi, J. Hombo, J. Am. Ceram. Soc. 76 (1993) 769.
[33] S. Böhm, R. Greef, H.N. McMurray, S.M. Powell, D.A. Worsley, J. Electrochem. Soc. 147 (9) (2000) 3286.
[34] F.B. Li, G.E. Thompson, J. Electrochem. Soc. 146 (5) (1999) 1809.
[35] J. Yu, J.C. Yu, M.K.-P. Leung, W. Ho, B. Cheng, X. Zhao, J. Zhao, J. Catal. 217 (2003) 69.
[36] D.R. Lide, Handbook of Chemistry and Physics, 81st ed., CRC Press, London, 2000–2001.
[37] J.-G. Yu, H.-G. Yu, B. Cheng, X.-J. Zhao, J.C. Yu, W.-K. Ho, J. Phys. Chem. B 107 (2003) 13871.
[38] T. Carnelley, J. Walker, J. Chem. Soc. (1888) 59.
[39] X. Yu, F. Li, X. Ye, X. Xin, J. Am. Ceram. Soc. 83 (4) (2000) 964.
[40] M. Ozawa, Scripta Mater. 50 (2004) 61.
[41] F.-B. Li, R.C. Newman, G.E. Thompson, Electrochim. Acta 42 (16) (1997) 2455.
[42] Y. Matsumoto, J. Hombo, C. Qiong, J. Electroanal. Chem. 279 (1990) 331.
[43] G.K. Williamson, W.H. Hall, Acta Met. 1 (1953) 22.